Decreasing Phanerozoic extinction intensity as a consequence of Earth surface oxygenation and metazoan ecophysiology

Richard G. Stockey[a,1], Alexandre Pohl[b,c], Andy Ridgwell[b], Seth Finnegan[d], and Erik A. Sperling[a]

[a]Department of Geological Sciences, Stanford University, Stanford, CA 94305; [b]Department of Earth and Planetary Sciences, University of California, Riverside, CA 92521; [c]Biogéosciences, UMR 6282, CNRS, Université Bourgogne Franche-Comté, F-21000 Dijon, France; and [d]Department of Integrative Biology, University of California, Berkeley, CA 94720

The decline in background extinction rates of marine animals through geologic time is an established but unexplained feature of the Phanerozoic fossil record. There is also growing consensus that the ocean and atmosphere did not become oxygenated to near-modern levels until the mid-Paleozoic, coinciding with the onset of generally lower extinction rates. Physiological theory provides us with a possible causal link between these two observations—predicting that the synergistic impacts of oxygen and temperature on aerobic respiration would have made marine animals more vulnerable to ocean warming events during periods of limited surface oxygenation. Here, we evaluate the hypothesis that changes in surface oxygenation exerted a first-order control on extinction rates through the Phanerozoic using a combined Earth system and ecophysiological modeling approach. We find that although continental configuration, the efficiency of the biological carbon pump in the ocean, and initial climate state all impact the magnitude of modeled biodiversity loss across simulated warming events, atmospheric oxygen is the dominant predictor of extinction vulnerability, with metabolic habitat viability and global ecophysiotype extinction exhibiting inflection points around 40% of present atmospheric oxygen. Given this is the broad upper limit for estimates of early Paleozoic oxygen levels, our results are consistent with the relative frequency of high-magnitude extinction events (particularly those not included in the canonical big five mass extinctions) early in the Phanerozoic being a direct consequence of limited early Paleozoic oxygenation and temperature-dependent hypoxia responses.

extinction | oxygen | ecophysiology | temperature-dependent hypoxia | Earth system evolution

One of the most striking and poorly understood features of the marine animal fossil record is a long-term decline in apparent extinction rates through the Phanerozoic (1–7). First revealed by analyses of stratigraphic range compilations around four decades ago (1), this decline has been a persistent feature in subsequent analyses using expanded databases (8) and improved extinction rate and richness metrics since then (e.g., refs. 2 to 7) (Fig. 1 and *SI Appendix*, Fig. S1). Declining genus-level extinction rates are a consistent feature of Phanerozoic analyses using a broad range of different richness and extinction rate metrics (7) (*SI Appendix*, Fig. S2 and Table S1) and are not substantially altered by varying temporal binning or controlling for species/genus ratio (*SI Appendix*, Figs. S1, S2 and Table S1 and *Materials and Methods*). In particular, the Cambrian and Ordovician periods stand out as intervals of especially high faunal turnover (6, 7, 9) (*SI Appendix*, Figs. S1 and S2), to the point that the early Paleozoic is often treated separately from the rest of the Phanerozoic in quantitative analyses of extinction (e.g., refs. 7, 10, 11). Changes in the distribution of lineage ages and geographic range sizes, area of continental shelf environments, intensity of species interactions, frequency of geological triggers, stabilization of Earth's climate, and rock area sampling biases have all been proposed as drivers of this trend (10–14). However, despite the long history of study and numerous proposed explanations, no consensus has been reached regarding the drivers of much higher early Paleozoic extinction rates versus those of the later Paleozoic, Mesozoic, and Cenozoic.

Secular trends in the oxygenation of the ocean and atmosphere are an underexplored factor that may help explain changing extinction intensity through time. A growing body of geochemical proxy evidence suggests that Earth's surface did not become oxygenated to near-modern levels until the early to mid-Paleozoic (Fig. 1) (15–20), and the most recent generation of long-term carbon cycle models support only limited early Paleozoic oxygenation (21–23). While early Paleozoic marine oxygen concentrations were self-evidently above minimum thresholds for aerobic metazoan metabolism (at least, in the shallow ocean), modern observations clearly show that variations in dissolved oxygen exert a strong control on marine biodiversity (24–26). Moreover, experimental respirometry, metabolic theory, and ecophysiological modeling have demonstrated that the synergistic effects of oxygen and temperature on the capacity for aerobic respiration significantly influence the metabolic viability of marine habitat (27–32). Following the principle of oxygen and capacity-limited thermal tolerance [OCLTT—see Pörtner (28) for review], the critical partial pressure of oxygen (pO_2) required to sustain resting metabolism increases exponentially with temperature, and the increase in oxygen supply required for ecologically sustainable populations results in a further steepening of this exponential

Significance

The decline in extinction rates through geologic time is a well-established but enigmatic feature of the marine animal fossil record. We hypothesize that this trend is driven largely by secular changes in the oxygenation of the atmosphere and oceans, as physiological principles predict that marine animals would have been more vulnerable to ocean warming during intervals of geological time with limited atmospheric oxygenation. We test this at a global oceanographic scale by combining models of ocean biogeochemistry and animal physiology. We show that atmospheric oxygen exerts a first-order control on the simulated extinction vulnerability of marine animals, highlighting its likely importance in controlling extinction trends through geologic time.
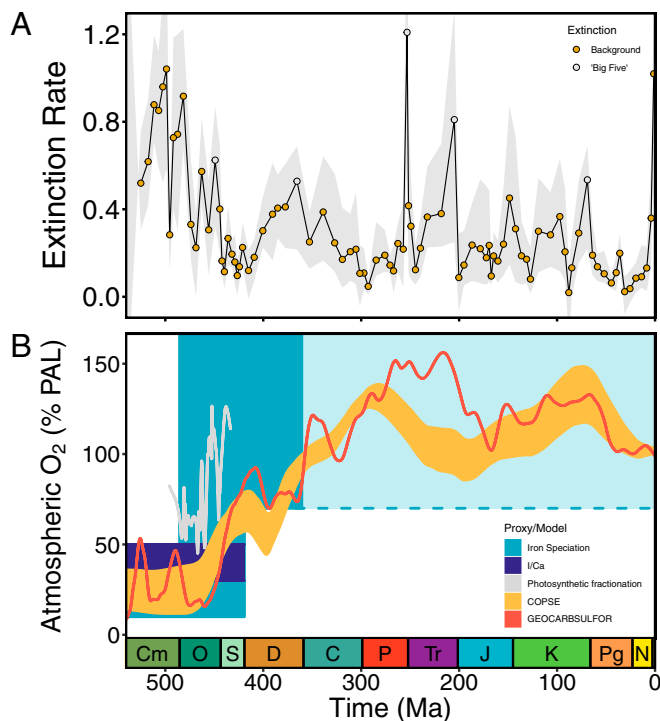
Fig. 1. Trends in extinction rates and atmospheric oxygen through the Phanerozoic. (*A*) Genus-level extinction rates for marine ectotherms [adapted from Kocsis et al. (7)] (*Materials and Methods*)—the line and points represent mean values, and the envelope represents maximum and minimum estimates from all 12 methodological approaches (three treatments: raw, classical rarefaction, and Shareholder Quorum Subsampling standardized; for each of four metrics: average per-capita rates, corrected three-timer rates, gap-filler rates, and second-for-third substitution rates). (*B*) Reconstructions of atmospheric oxygen from biogeochemical models (21, 22, 78) and geochemical proxy records (15, 17). Records for photosynthetic fractionation (78) and COPSE (22) biogeochemical models were generated by fitting cross-validated local regression (LOESS, locally estimated scatterplot smoothing) models to published data.

relationship (Fig. 2) (33). Meta-analyses investigating the sensitivity of modern marine ectotherms to climate-related stressors and the vulnerability of their fossil representatives to extinction further suggest that physiological traits of modern marine animals can be generally scaled to extinction sensitivity to ancient climate perturbations (34).

Seawater pO_2 would have been dramatically lower in an early Paleozoic Earth system with limited surface oxygenation, leading to the prediction that marine ectotherms would have been substantially more vulnerable to temperature-dependent hypoxia, and therefore climate-driven extinction, due to reduced thermal safety margins in poorly oxygenated ancient oceans (Fig. 2) (35). This logic further leads to the implication that dissolved oxygen was likely important to the structure of marine ecosystems at concentrations well above critical hypoxic thresholds that have previously been invoked for the evolution of early animals (36, 37), as is observed at regional scales in modern marine environments (29–31, 38). Recent advances in Earth system modeling provide an opportunity to test this hypothesis at the planetary scale and to explicitly distinguish the role of changes in surface oxygenation through the Phanerozoic from variations in continental configuration, biological carbon cycling, and climate state.

Our approach is twofold—incorporating both Earth system and ecophysiological modeling. First, using an Earth system model of intermediate complexity [cGENIE (39)—see *Materials and Methods* and *SI Appendix*] and an ensemble experimental

approach, we generate a suite of three-dimensional realizations of potential marine environmental conditions. These Earth system model experiments span a range of scenarios for atmospheric O_2 and CO_2 concentrations (Fig. 3*A*) in order to address uncertainty associated with reconstructions of these variables through geologic time (e.g., Fig. 1*B*). Atmospheric CO_2 concentrations are varied to force global climate in our experiments, and solar forcing is kept constant for each ensemble (Fig. 3). Simulating the potential three-dimensional (3D) structure of past oceans in these experiments is critical: in the upper ocean, oxygen and temperature both decrease with depth but have opposite gradients with respect to latitude (33, 38). Temperature gradients decrease toward the poles, while subsurface oxygen gradients increase. Because aerobic habitability for marine animals involves the synergistic combination of oxygen and temperature (29, 34, 35, 38), elucidating the spatial complexity of the environmental landscape of ancient oceans is required to appropriately understand biological responses to environmental perturbations.

We additionally identify key boundary conditions that have significantly changed through Earth history and may offer alternative explanations for the trends in extinction rates observed in the fossil record: 1) continental configuration, which affects latitudinal habitat (i.e., continental shelf) distribution as well as ocean circulation (and resulting temperature and oxygen gradients) and could therefore have modulated the susceptibility of animals to extinction (33, 40, 41); 2) the efficiency of the biological carbon pump in the ocean, which exerts a control on the distribution of oxygen in the upper water column (42) and has been previously identified as important in differentiating earlier Paleozoic versus Mesozoic–Cenozoic ocean redox conditions (17); and 3) climate state, which directly impacts ocean surface temperatures (and by extension dissolved marine oxygen) and therefore influences how close animals at a given latitude are living to their physiological limits (29, 38).

Utilizing model ocean temperatures and dissolved oxygen concentrations from this suite of 3D realizations, we then employ the recently developed Metabolic Index (29, 33, 38) in order to evaluate the proportion of modern marine ectotherms (based upon available experimental respirometry data) that could survive in these simulated environments. While we do not attempt to directly simulate taxonomic diversity, the Metabolic Index provides us with a means to mechanistically assess the physiological ecotypes (herein, ecophysiotypes) that can contribute to biodiversity. We apply a probabilistic representation of temperature-dependent hypoxia responses (Fig. 2) to define "metabolic habitat viability," a global metric describing the percentage of feasible ecophysiotypes that can live anywhere in the shelf environments of our 3D ocean models. Following other paleoecological modeling approaches (e.g., ref. 41), we focus our analyses on shelf environments because they constitute the majority of the Phanerozoic fossil record and host the majority of marine biodiversity in the modern oceans, although we provide complementary simulations for the entire global ocean.

Finally, we estimate global extinction sensitivity to warming across a range of atmospheric O_2 concentrations to link our ecophysiological models more directly to the trends we observe in the geologic record. We model "global ecophysiotype extinction" as the predicted loss of ecophysiotypes across a nominal warming event of ~5 °C (as defined by mean temperature change in the equatorial surface ocean; *SI Appendix*, Fig. S3 and Table S2). These warming events are represented by Earth system models separated by two doublings of atmospheric CO_2 and are designed to mimic relatively extreme (but not infrequent) examples of climate variability known to have occurred throughout Earth history (43, 44). We performed this extinction sensitivity estimate for all scenarios of atmospheric O_2 and for each ensemble (testing the impacts of continental configuration and biological pump efficiency; Fig. 3 and *SI Appendix*, Fig. S3) across multiple baseline
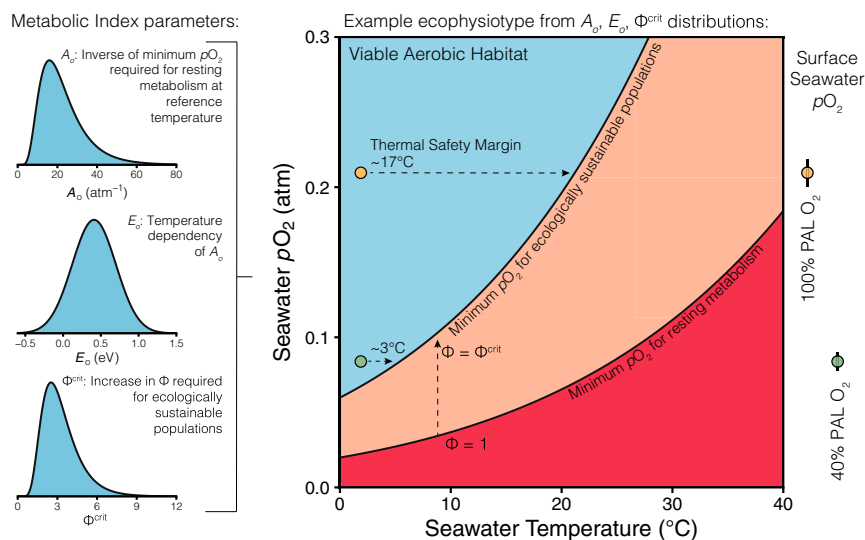
Fig. 2. Schematic of ecophysiological model based on the Metabolic Index (Eq. **1**). (*Left*) The frequency distributions of three key ecophysiological parameters—A_o, E_o, and ϕ^{crit}—are illustrated. (*Right*) The implications of these parameters for the ecophysiological modeling framework employed in this study are illustrated for an example ecophysiotype based on the median values of these distributions. The minimum seawater pO_2 required for resting metabolism increases at an exponential rate primarily because of temperature effects on metabolic rate. The minimum seawater pO_2 required for sustainable populations on ecological timescales also increases exponentially with temperature (faster than the minimum pO_2 required for resting metabolism) as the product of an exponential function defined by A_o, E_o, and ϕ^{crit} (see *Materials and Methods* and Eq. **1** for full details). At a given temperature, the thermal safety margin of a hypothetical ecophysiotype is predicted to decrease with decreasing seawater pO_2 (either because of a change in equilibrium oxygen levels resulting from decreasing atmospheric oxygen or a decrease in saturation resulting from biogeochemical processes such as organic carbon remineralization). Surface seawater pO_2 distributions (far *Right*) are taken from Earth system model analyses presented in this study (8 PAL CO_2 Ordovician configuration; points represent mean values and error bars 2 SD).

climate states. We further explore the consistency of our results across different thresholds for minimum habitat area (number of equal area ocean model cells) and tolerances for proportional habitat loss, as well as across deviations from the distributions of physiological tolerances observed in modern marine ectotherms. Thus, by combining ecophysiology and ensemble Earth system

modeling, we evaluate the vulnerability of marine ectotherms to warming events at a range of atmospheric O_2 levels in a framework that is neutral to the selective advantage of different ecophysiotypes and explores the relative impacts of other aspects of Phanerozoic Earth system evolution on marine animal ecophysiology.
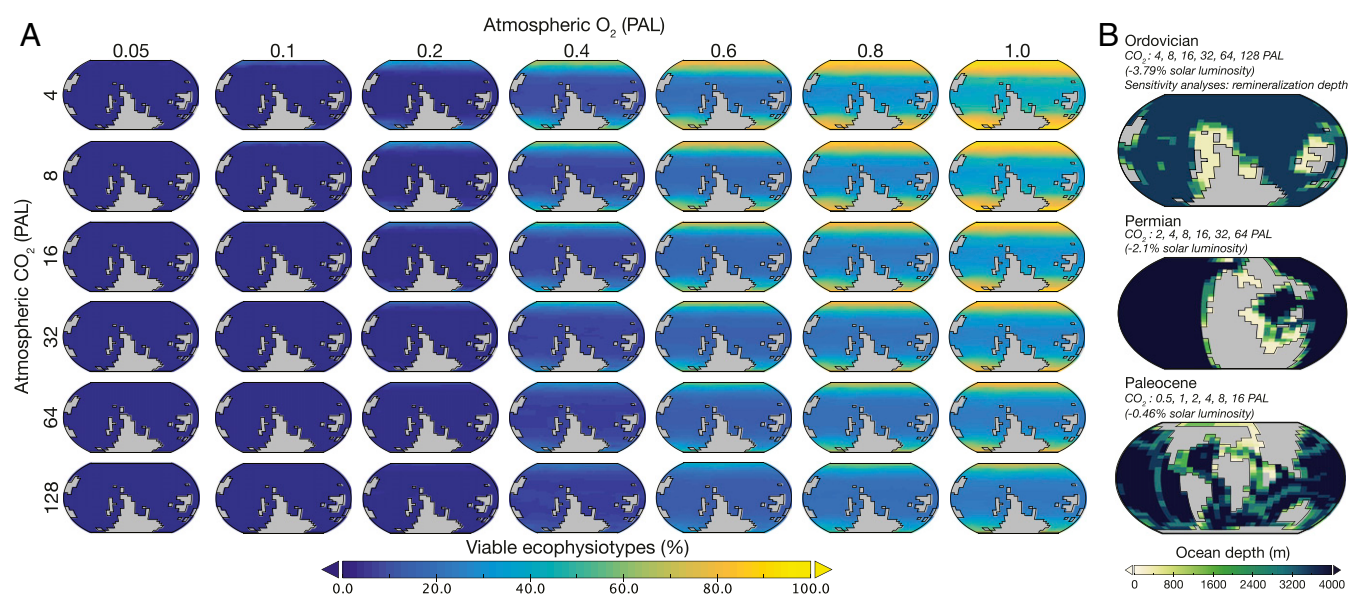

Fig. 3. Ensemble Earth system modeling approach using cGENIE. (*A*) Example of ensemble O_2–CO_2 Earth system modeling experiment using Ordovician continental configuration with modern remineralization depth. Color scale illustrates the proportion of the modeled ecophysiotypes that can live in each cell of the surface ocean (top 0- to 80-m layer of the 16-layer cGENIE ocean is illustrated here). (*B*) Sensitivity analyses performed in this study. Variations in continental configuration, remineralization depth, and CO_2 forcing are detailed here. The atmospheric O_2 levels investigated in each ensemble experiment are the same. We present full surface ocean models here for ease of visual comparison, although main text analyses use only nonpolar shelf environments (as illustrated in *SI Appendix*, Fig. S3).
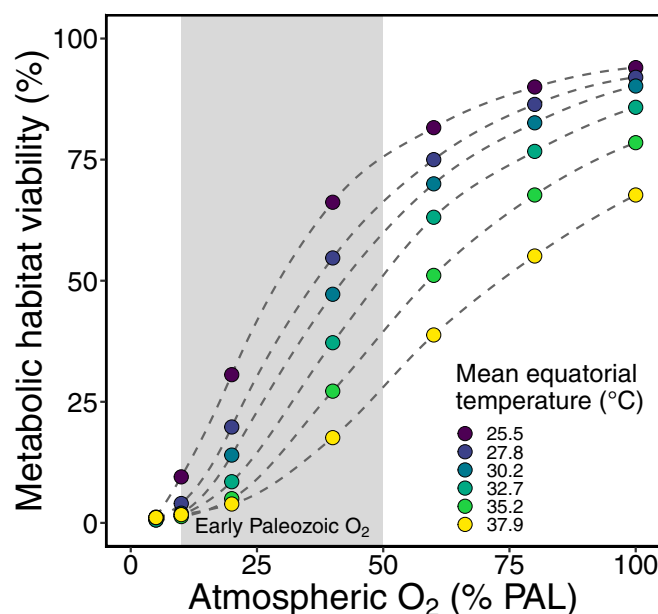
Stockey et al.
Decreasing Phanerozoic extinction intensity as a consequence of Earth surface oxygenation and metazoan ecophysiology

PNAS | 3 of 8
https://doi.org/10.1073/pnas.2101900118

Fig. 4. Metabolic habitat viability for the ensemble O_2–CO_2 Earth system modeling experiment with an Ordovician continental configuration and modern remineralization depth. Metabolic habitat viability is calculated as the proportion of the ecophysiotypes modeled that can live in shelf environments of each 3D ocean model produced using cGENIE (*Materials and Methods*). Circles represent individual experiments and are color-coded by mean equatorial sea surface temperature (−3.2° S to 3.2° N, 0 to 80 m depth) as a product of atmospheric CO_2 forcing.

Results

Metabolic Habitat Viability. Metabolic habitat viability—the total number of ecophysiotypes that can live in the shelf environments of each ancient ocean realization—is shown in Fig. 4 for our ensemble of simulations employing an Ordovician continental configuration and *SI Appendix*, Fig. S4 for all other Earth system model ensembles. In all ensembles, metabolic habitat viability exhibits a positive relationship with atmospheric O_2 and a negative relationship with global temperature, resulting in a sigmoidal relationship between atmospheric O_2 and metabolic habitat viability for a given climate state. While our primary analyses focus on shelf environments, very similar trends are observed when the entire ocean is considered as a potential habitat for marine animals (*SI Appendix*, Figs. S5 and S6). Using entire 3D ocean models often results in slightly higher estimates of metabolic habitat viability because cooler and (at higher atmospheric O_2 levels) well-oxygenated deep ocean environments may act as refugia, despite being unlikely diversity hotspots for other reasons such as food supply (45, 46). The latitudinal distribution of viable ecophysiotypes is similar between continental configurations (Fig. 3 and *SI Appendix*, Fig. S3), with more ecophysiotypes generally able to inhabit cooler polar regions of the surface ocean. Identifying oceanographic and tectonic drivers of regional differences in viable ecophysiotype biogeography between continental configurations is an interesting avenue for future research, but this would require tuning model ensembles to precisely equivalent climate states and is therefore beyond the scope of this study.

Changes in metabolic habitat viability between cooler and warmer climate states allow us to begin linking ecophysiology to extinction sensitivity under different scenarios of atmospheric oxygenation (Fig. 4). The percentage change in metabolic habitat viability between colder and warmer ocean simulations increases as atmospheric oxygen decreases from modern levels (100% preindustrial atmospheric levels [PAL]), reaching maximum

values at atmospheric O_2 concentrations reconstructed for the early Paleozoic (<40 to 50% PAL—gray envelope in Fig. 4 and *SI Appendix*, Fig. S4). Furthermore, because extinction is expected to track the proportional rather than absolute loss of ecophysiotypes (33, 34), differences in metabolic habitat viability would therefore be amplified to result in high levels of warming-driven extinction at lower levels of atmospheric oxygenation reconstructed for the early Paleozoic (e.g., 20% PAL). In such cases, the number of viable ecophysiotypes in any low-O_2 scenario is much lower, leading to greater proportional change despite a similar absolute change in metabolic habitat viability to that predicted at higher O_2 levels (e.g., 80% PAL). Our analyses thus demonstrate that the expected proportional loss of ecophysiotypes during a global warming event would be substantially higher under the limited surface oxygenation scenarios hypothesized for the early Paleozoic than for modern (or, more broadly, post mid-Paleozoic) levels of oxygenation.

Sensitivity of Global Extinction Simulations. When we simulate the impacts of warming events on the extinction of marine animals, the general trend of greater predicted extinction at lower atmospheric oxygen levels is a common feature of all ensemble experiments (Fig. 5 and *SI Appendix*, Figs. S7–S12). There is variation in the absolute magnitude of simulated global ecophysiotype extinction between the different continental configurations tested in our ensembles. However, we do not observe any time-dependent trends in extinction sensitivity between progressive continental reconstructions, and the most striking feature of the results remains the nonlinear increase in global ecophysiotype extinction with declining oxygenation (Fig. 5 and *SI Appendix*, Figs. S7–S12). Below 10% PAL O_2, the relationship between modeled extinction and atmospheric oxygen is less
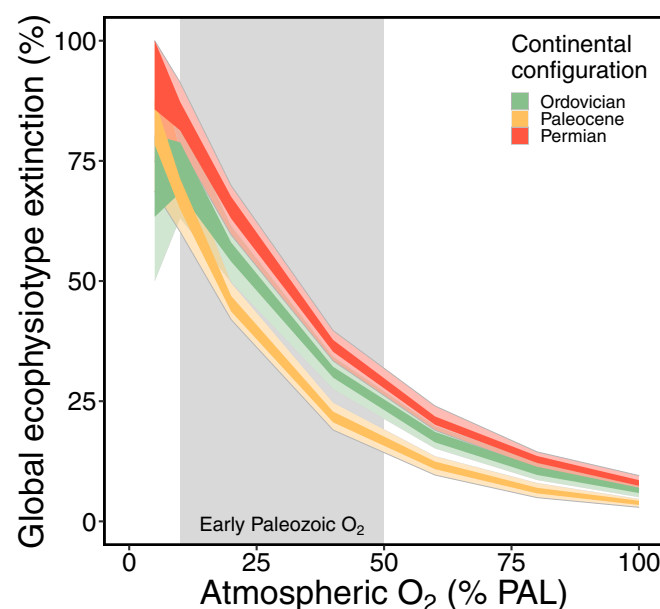

Fig. 5. Global ecophysiotype extinction predicted to result from an ∼5 °C warming event from an approximately preindustrial baseline sea surface temperature at different atmospheric O_2 levels, illustrating sensitivity analyses evaluating the influence of continental configuration on predicted extinction. Global ecophysiotype extinction is defined as the proportion of ecophysiotypes that were viable in the shelf environments of the colder baseline simulation but are no longer viable in any cell of the shelf environments of the warmer ocean simulation (*Materials and Methods*). Baseline CO_2 levels used: 1 PAL, Paleocene; 8 PAL, Permian; and 8 PAL, Ordovician. Darker envelopes represent 25th to 75th percentiles of 100 simulation results, and lighter envelopes represent 5th to 95th percentiles.

predictable. However, the initial pool of viable pre-extinction ecophysiotypes in these simulations is very small at low O$_2$ levels (Figs. 3 and 4 and *SI Appendix*, Figs. S4–S6), suggesting that this inconsistency may partially be a product of sample size (as supported by wider envelopes in Fig. 5 and *SI Appendix*, Fig. S7, S8, and S11) and the limited experimental respirometry data for animals that live in low-oxygen environments (47). We find that modeled extinction is high at low atmospheric oxygen levels for the Ordovician configuration regardless of the efficiency of the biological pump (*SI Appendix*, Fig. S7), suggesting that despite its role in controlling the distribution of oxygen in the upper water column, this factor is of secondary importance for extinction compared to atmospheric O$_2$. A shallower remineralization depth does slightly reduce simulated extinction sensitivity at low atmospheric O$_2$ (~5 to 20% PAL), although the same caveat of small initial ecophysiotype population size applies.

Increasing the baseline temperature in our extinction simulations (i.e., testing for any initial climate state dependence of extinction susceptibility) results in increased predicted global ecophysiotype extinction for all three continental configurations (*SI Appendix*, Fig. S8). A corresponding decrease in modeled ecophysiotype extinction is generally observed at cooler baseline temperatures. Cool, low-O$_2$ (≤20% PAL) Ordovician simulations are a minor exception to this general rule, suggesting that continental configuration may exert a second-order control on the climate state dependence of extinction vulnerability. The impact of initial climate state on simulated ecophysiotype extinction appears less dramatic than the impact of atmospheric oxygen, particularly in light of the apparent inflection in modeled extinction observed around upper estimates for early Paleozoic O$_2$ levels. However, we note that pre-extinction climate state impacts modeled ecophysiotype extinction more than any other Earth system boundary condition explored in our sensitivity analyses.

Altering the assumptions of our ecophysiological modeling approach does not dramatically impact the observed relationship between predicted extinction and atmospheric oxygen. In our primary analyses, we define ecophysiotype extinction as only occurring when no cells in our simulated shelf environments are viable for an ecophysiotype or (equivalently) when 100% of metabolically viable habitat area is lost. Increasing the minimum number of inhabited ocean cells required to survive a warming event or decreasing the proportional habitat loss required for extinction moderately increases modeled global ecophysiotype extinction (*SI Appendix*, Figs. S9 and S10). The differences in the shape of these responses highlight the importance of these parameters and the second-order effects of continental configuration. However, the overall trend of decreasing extinction intensity with increased atmospheric O$_2$, with an apparent inflection point generally around 40% PAL, is consistent across all of these simulations. Similar trends are observed when investigating the impacts of varying the distributions used to parameterize physiological responses (A_o, the inverse of the hypoxic threshold at a reference temperature, and E_o, the temperature dependency of the hypoxic threshold). While varying the distributions of A_o and E_o does impact the magnitude of simulated global ecophysiotype extinction and the steepness of the inflection around 40% PAL O$_2$ (*SI Appendix*, Fig. S11), the overarching trends of increasing predicted extinction with decreasing atmospheric oxygen (down to at least 20% PAL O$_2$) are not impacted. The size of the synthetic population of ecophysiotypes (*Materials and Methods*) has no noticeable effect on the analyses illustrated in Fig. 5 (*SI Appendix*, Fig. S12).

Discussion

Using a coupled Earth system and ecophysiological modeling approach, our analyses suggest that oxygenation of the shallow ocean (as modulated by atmospheric oxygen levels) is the dominant factor in governing the vulnerability of marine animals to extinction during warming events through geologic time. These results remain consistent when complex oceanographic relationships between temperature and seawater oxygenation and uncertainties in ocean circulation, biological pump efficiency, climate state, and habitat area thresholds are taken into account. Critically, the relationship we observe between simulated global ecophysiotype extinction and atmospheric oxygen is nonlinear, with an apparent inflection point around 40% PAL O$_2$ (Fig. 5). This broadly coincides with the upper limit of estimates for early Paleozoic atmospheric oxygen (Fig. 1) (15, 17), supporting the hypothesis that relatively low atmospheric oxygen levels created boundary conditions under which high-magnitude extinction events were more likely to occur as a product of climate variability.

While atmospheric oxygen is the primary control on extinction sensitivity in our simulations, our analyses show that other factors modulate the response to varying degrees. This is unsurprising considering how these factors affect the 3D oxygen–temperature landscape of the ocean. In particular, our analyses indicate that continental configuration may play an important secondary role in governing ecophysiotype extinction vulnerability at the global scale (Fig. 5), although this is difficult to clearly separate from minor climatic differences between ensembles. Notably, we do not observe time-correlative trends between the three continental configurations that could help explain the secular extinction rate observations from the fossil record. In other words, we do not find that extinction sensitivity in the polar-biased and relatively compact continental configuration of the Ordovician is particularly different from that of the more evenly latitudinally distributed and dispersed configuration of the Paleocene when compared to the differences associated with changing atmospheric O$_2$. The efficiency of the biological pump (simulated here as a difference in prescribed remineralization depths in the ocean) is also thought to have changed through the Phanerozoic (17). However, we find that the differences in simulated extinction sensitivity are minimal and (if anything) in opposition to the influence of changes in atmospheric oxygenation (*SI Appendix*, Fig. S7). This is likely because both continental configuration and carbon remineralization depth mainly change oxygen distributions in the deeper ocean, whereas most animals are living (and dying) in the surface ocean, which is closely coupled to the O$_2$ concentration of the atmosphere. Finally, while the habitat area thresholds we used to define simulated extinction and the specific parameterization of physiological traits do impact the slope and magnitude of the observed relationship between atmospheric oxygen and extinction (in expected directions; *SI Appendix*, Figs. S9–S11), the first-order trends remain consistent regardless of how we parametrize our ecophysiological extinction model.

We additionally find that an important climate state dependence exists for ecophysiological extinction sensitivity. Marine animals are expected to be living closer to their thermal limits as defined by OCLTT in warmer environments based on observations from modern tropical marine habitats (Fig. 2) (29, 38), with implications for broader areas of the ocean in ancient greenhouse climates. We provide further model support for this hypothesis by demonstrating increased simulated extinction magnitudes in warmer climate states (*SI Appendix*, Fig. S8). Very warm early Paleozoic sea surface temperatures have been reconstructed using geochemical paleothermometry (48–50), suggesting that this phenomenon could also provide some explanatory power for the frequency of high-magnitude extinctions. However, while recent advances in paleothermometry have shown considerable potential in constraining Ordovician climate dynamics (50), there is still currently limited consensus on directional trends in early Phanerozoic sea surface temperatures, especially in the earliest Paleozoic (51–53). In contrast, reconstructions of atmospheric oxygen are increasingly consistent, even if the absolute concentrations are poorly constrained (Fig. 1). This discussion should also not be framed as a question of oxygen versus temperature; inherent to the concept of temperature-dependent hypoxia is that both interact to

Stockey et al.
Decreasing Phanerozoic extinction intensity as a consequence of Earth surface oxygenation and metazoan ecophysiology

PNAS | 5 of 8
https://doi.org/10.1073/pnas.2101900118

determine aerobic safety margins (Fig. 2) (29, 34, 38). We therefore suggest that atmospheric oxygen can confidently be established as a first-order control on early Phanerozoic extinction rates and that potentially high sea surface temperatures through the same time interval may have amplified the effect of limited surface oxygenation. Changes in the latitudinal focus of fossil sampling through the Phanerozoic may also bias extinction rate estimates slightly toward environments with warmer baseline temperatures in the early Paleozoic when well-sampled paleocontinents were mainly situated at low latitudes (54). However, the lack of similarly high long-term extinction rates across other intervals with low-latitude sampling biases indicates that this cannot fully explain the trends we seek to explain here and that atmospheric oxygen (potentially compounded by warm global climate) is a more probable first-order driver.

The plausibility of temperature-dependent hypoxia as a driver of high early Paleozoic extinction rates is supported by links between sea level changes, ocean deoxygenation, and extinctions during this interval of geologic time. The Cambrian–Ordovician biomere-style extinction events are a major component of the characteristically high early Paleozoic extinction rates (9). These events, predominantly observed in the trilobite fossil record (e.g., ref. 55), have long been recognized as associated with sedimentological evidence of sea level change, possible thermocline migration, and ocean anoxia (56, 57). Stable isotope geochemistry provides further evidence that the biomere events were linked to major marine carbon and sulfur cycle perturbations, consistent with ocean warming and deoxygenation (58–61). Similar inferences of ocean anoxia and rapid sea level change have been made for the early Cambrian Botomian extinction event (62). In contrast, multiple Mesozoic and Cenozoic hyperthermals (including the Paleocene–Eocene Thermal Maximum and Cretaceous Oceanic Anoxic Event 2) that exhibit similar broad patterns of environmental change (43, 63–65) do not correlate with global marine extinctions of comparably high magnitude (Fig. 1) (7, 9). Our analyses demonstrate that the effects of changing atmospheric oxygenation on the thermal safety margins of marine ectotherms (Fig. 2) may account for this discrepancy in extinction magnitude between events with similar signatures of environmental change. Our simulations of metabolic habitat viability also offer a potential mechanism for the high origination rates observed through the early Paleozoic (6, 7)—particularly if simple logistic models of extinction and subsequent recovery (i.e., origination, e.g., refs. 4, 66) can be broadly applied to the Phanerozoic fossil record. However, we focus on warming-driven extinction events because fewer assumptions regarding the evolutionary advantages of different ecophysiotypes (and how they relate to the rate at which physiological diversity increases in cool climate states) are required for these models, which simply simulate the instantaneous loss of viable ecophysiotypes.

Our combined Earth system and ecophysiological modeling approach provides a methodological advance in moving from simple correlations to a more mechanistic understanding of how environmental change impacted marine ecosystems through Earth history. The use of physiology as a conceptual bridge between the fossil and geochemical records is of clear appeal for establishing the mechanistic drivers of animal–environment interactions from the geologic record (67). However, the power of Earth system models in simulating the ecophysiological responses of marine animals to deep-time environmental change is only recently being explored (e.g., refs. 33, 41). We apply simple assumptions about the diversification of ecophysiotypes (i.e., that ecophysiotypes proliferate in times of stability and become inviable during warming events) to test the hypothesis that limited atmospheric oxygenation would increase physiological vulnerability to ocean warming events on geologic timescales. For increasingly accurate models of animal–environment interactions through the Phanerozoic (for example, ones that directly simulate

latitudinal gradients in taxonomic diversity), other key variables involved in these interactions will need to be incorporated. At the organism scale, physiological traits including vulnerability to ocean acidification, food supply limitation, and possible variations in physiological responses are all likely important variables. For example, the different buffering capacities of marine animal groups have previously been invoked to explain differential extinction selectivity (68, 69). Meta-analytical approaches also suggest that sensitivity to climate-related stressors correlates with genus survival across ancient extinction events in higher-level taxonomic groups (34), further indicating that differences in physiological tolerances between marine clades may be an important consideration when applying ecophysiological principles to Earth history. While we demonstrate that our results are consistent across a range of deviations from mean modern physiological responses, it will hopefully become feasible to begin linking physiological traits more directly to extinct animal groups based on phylogenetic and adaptive principles as the availability of experimental respirometry data characterizing temperature-dependent hypoxic responses of marine ectotherms increases. At the macroecological scale, migration [as applied in Saupe et al. (41)], species interactions, and resource competition also play key roles in governing population and species responses to environmental change. As model frameworks for deep-time animal–environment interactions develop in terms of both ecophysiological and biogeochemical realism, the temporal–spatial resolution of paleontological and geochemical databases will also be critical to the explanatory power of these methodologies, as will techniques addressing the limitations and biases inherent to the geologic record (4–6, 13, 54, 70–72).

Conclusions

Using an ensemble Earth system and ecophysiological modeling framework, we demonstrate that atmospheric oxygen levels likely exerted a first-order control on extinction vulnerability through the Phanerozoic. Our model analyses illustrate that the theoretical predictions of OCLLT are expected to have globally significant implications, resulting in dramatically increased extinction of marine animals under varying climatic conditions during geological periods with limited surface oxygenation. While warmer initial climate states increase the magnitude of our simulated extinctions, and continental configuration and the strength of the biological pump also have minor impacts on our predictions, the trend of increased extinction vulnerability with early Paleozoic levels of atmospheric oxygen is dominant across all of our simulations. We therefore argue that the exceptional frequency of high-magnitude extinction events in the early Paleozoic was primarily a consequence of limited surface oxygenation and temperature-dependent hypoxia responses in marine animals.

Materials and Methods

Quantitative Paleobiology. We performed a series of quantitative paleobiological analyses to evaluate evidence for declining extinction rates through the Phanerozoic. We adapted methods from Kocsis et al. (7) to generate reconstructions and statistical analyses of extinction rates through the Phanerozoic specifically for marine ectotherms. For these analyses, we used an updated download of fossil occurences from the Paleobiology Database (PBDB) (8) and omitted endothermic and/or exclusively air-breathing higher-level marine taxa (marine mammals, marine reptiles, and turtles). This PBDB data was downloaded on June 22, 2021 using the same specifications as Kocsis et al. (7) and is archived on GitHub. We generated reconstructed extinction rates using three richness metrics (classical rarefaction, raw occurrences, and shareholder quorum subsampling) and four extinction rate metrics (second-for-third substitution, corrected three timer, gap filler, and per capita). We applied these metrics to generate reconstructions for all genera both at stage resolution and using the PBDB ~10-million-year bins. To investigate the potential impact of changing species to genus ratios through the Phanerozoic (e.g., ref. 73), we further conducted the same analyses on filtered datasets, generating reconstructions for all genera, genera with a single accepted named species, genera with two species, genera with three species, and genera with four or more accepted named species (*SI Appendix*, Fig. S1). For

shareholder quorum subsampling analyses, we used a quorum level of 0.5 to accommodate lower sampling intensity in filtered datasets [as supported by Boag et al. (32)] and remain within the >0.4 quorum range suggested by previous authors (7). Fig. 1 is a summary of the top right panel of *SI Appendix*, Fig. S1, including all genera at stage resolution. We further fit cross-validated LOESS (locally estimated scatterplot smoothing) models to our reconstructed extinction rates to evaluate whether early Paleozoic decreases in extinction rates were a major feature of the full Phanerozoic record (*SI Appendix*, Fig. S2). Finally, we generated Spearman's correlation coefficients to investigate the statistical significance of temporal declines in extinction rates across all of our treatments (*SI Appendix*, Table S1). The adapted code from Kocsis et al. (7) and filtered PBDB download are available at https://github.com/richard-stockey/cGENIE-metabolic_index.extinction and are assigned a DOI: 10.5281/zenodo.5519730.

Earth System Modeling.

cGENIE is an Earth system model of intermediate complexity designed for the spatially explicit biogeochemical characterization of global-scale paleoceanographic problems (39). We create a range of 3D realizations of ocean environmental conditions by running ensembles of model experiments. The experiments in each ensemble are run for 10,000 or 20,000 y (depending on the time required for dissolved marine O_2 and seawater temperature to reach steady state). We used a range of assumptions regarding atmospheric pCO_2 specific to each continental configuration based on changing solar luminosity and albedo (Fig. 3), and a range of atmospheric pO_2 scenarios based on the range of estimates from geochemical proxy data and biogeochemical box modeling (Fig. 1). We apply this ensemble treatment to three ancient continental configurations, chosen for their relatively even temporal spread across the Phanerozoic and history of use in previous paleoclimate studies—a Paleocene configuration (~55 Ma) (43), a Permian configuration (~251 Ma) (74), and an Ordovician configuration (~450 Ma) [based on the 8 PAL CO_2 FOAM (Fast Ocean Atmosphere Model) simulation of Pohl et al. (75)—*SI Appendix*]. For each of these ancient configurations, we apply age-appropriate solar luminosity (76). Finally, in the Ordovician continental configuration we explore the possible influence of postulated Phanerozoic changes in organic matter remineralization depth in the ocean (17, 42)—testing ~1/3 modern, or specifically 200 m, e-folding depth (42).

We extract the mean annual ocean temperature and ocean oxygen concentration during the last simulated year for each ocean grid cell and generate corresponding seawater oxygen partial pressure (pO_2) values [following the methods of Hofmann et al. (77)]. Changing solar luminosity and continental configuration results in different mean sea surface temperatures for the same atmospheric CO_2 assumption. We therefore identify the pCO_2 values for each continental configuration that create comparable climate simulations (*SI Appendix*, Table S2). These climate scenarios are compared using the mean equatorial (3.2° S to 3.2° N, 0 to 80 m depth) surface ocean temperature for each model (Fig. 4 and *SI Appendix*, Figs. S4–S6 and Table S2).

The code for the version of the "muffin" release of the cGENIE Earth system model used in this paper is tagged as v0.9.19 and is assigned a DOI: 10.5281/zenodo.4473048. Configuration files for the specific experiments presented in the paper can be found in the directory genie-userconfigs/MS/stockeyetal.PNAS.2021. Details on the experiments, plus the command line needed to run each one, are given in the readme.txt file in that directory. All other configuration files and boundary conditions are provided as part of the code release.

A manual detailing code installation, basic model configuration, and tutorials covering various aspects of model configuration, experimental design, and output, plus the processing of results, is assigned a DOI: 10.5281/zenodo.4469678.

Ecophysiological Simulations of Animal–Environment Interactions.

We combine our ensemble Earth system modeling experiments with a probabilistic ecophysiological model of extinction vulnerability. The Metabolic Index, as defined by Deutsch et al. (29) and Penn et al. (33), is configured here to calculate the proportion of modern marine ectotherms (based on described temperature-dependent hypoxia responses) that can inhabit each ocean cell in the cGENIE Earth system model.

$$\text{Metabolic habitat viability} = \sum_{\min(A_o, E_o, \phi^{crit})}^{\max(A_o, E_o, \phi^{crit})} A_o \frac{pO_2}{\exp\left[\frac{-E_o}{k_B}\left(\frac{1}{T} - \frac{1}{T_{ref}}\right)\right]} > \phi^{crit} \quad [1]$$

At the individual organism scale, A_o is the inverse of the hypoxic threshold of the organism (the minimum required seawater pO_2 [P_{crit}] to sustain resting

aerobic metabolism) at a reference temperature T_{ref}, E_o is the temperature dependency of the hypoxic threshold, and ϕ^{crit} is the multiplicative increase in oxygen supply that is required to support ecologically sustainable populations (calculated based on biogeographic distribution, relative to experimental respirometry measurements of resting metabolism). In our modeling approach, these variables are parametrized by probability density functions based on observations from laboratory experiments and species distributions [Fig. 2; following Penn et al. (33)]. Seawater temperature and pO_2 are environmental variables generated through the Earth system modeling approach described above (Fig. 3). All other variables are constant (k_B is the Boltzmann constant, and T_{ref} is a reference temperature of 15 °C). In our analyses, we simulate 1,000 ecophysiotypes, sampled from probability distributions of A_o, E_o, and ϕ^{crit} and map which cells (if any) in each cGENIE ocean model are habitable for each ecophysiotype (see *SI Appendix*, Fig. S12 for exploration of the number of ecotypes used).

Metabolic habitat viability, as defined here, quantifies the proportion of these modeled ecophysiotypes that can live in the nonpolar shelf environments (defined as any cell adjacent to continental land mass in the top three layers of the cGENIE ocean, or <283.8 m water depth) of each global ocean model. See *SI Appendix*, Figs. S5 and S6 for sensitivity analyses using the entire global ocean model rather than shelf environments alone. Polar environments (>70° N and >70° S) are excluded from all analyses due to the coarse model resolution of polar ocean environments (e.g., in a Paleocene northern polar ocean) in cGENIE and to reduce local nonlinear responses to sea ice extent.

We further simulate extinction as the global loss of ecophysiotypes between two CO_2 scenarios at the same O_2 level. Specifically, we evaluate the proportional loss of ecophysiotypes between baseline climate states (relatively cool, approximately preindustrial mean equatorial surface ocean temperatures, *SI Appendix*) and equivalent model scenarios that have undergone ~5 °C equatorial warming (*SI Appendix*, Table S2). We therefore model a nominal hyperthermal event of roughly the same magnitude as the Paleocene–Eocene Thermal Maximum (43) at each atmospheric O_2 level. Global ecophysiotype extinction is thus defined as the proportion of ecophysiotypes that were viable in shelf environments of the colder baseline simulation but are no longer viable in any continental shelf cell of the warmer ocean simulation. Sensitivity analyses exploring the number of viable cells required to survive a simulated warming event, and the proportional habitat loss required to drive extinction, are shown in *SI Appendix*, Figs. S9 and S10. Additional sensitivity analyses exploring deviations from the distributions of A_o and E_o defined in Penn et al. (33) are shown in *SI Appendix*, Fig. S11. In these analyses, "low" and "high" distributions have mean values defined by the 25th and 75th percentiles of the distributions used in our primary analyses and half of the variance of those distributions. In plots of global ecophysiotype extinction in shelf environments (e.g., Fig. 5), we summarize the distribution of results from 100 different simulated populations of 1,000 randomly sampled ecophysiotypes to illustrate the range of sampling-related uncertainty in our probabilistic approach to ecophysiological modeling. All plots of single ecotype populations (i.e., those with points rather than envelopes, Fig. 4 and *SI Appendix*, Figs. S4–S6) use the same randomly sampled population.

R scripts to reproduce the ecophysiological analyses and associated figures are available at https://github.com/richardstockey/cGENIE-metabolic_index.extinction and are assigned a DOI: 10.5281/zenodo.5519730.

Stockey et al.
Decreasing Phanerozoic extinction intensity as a consequence of Earth surface oxygenation and metazoan ecophysiology

PNAS | 7 of 8
https://doi.org/10.1073/pnas.2101900118

1. D. M. Raup, J. J. Sepkoski Jr, Mass extinctions in the marine fossil record. *Science* **215**, 1501–1503 (1982).

2. M. Foote, Origination and extinction components of taxonomic diversity: General problems. *Paleobiology* **26**, 74–102 (2000).

3. M. Foote, Origination and extinction through the Phanerozoic: A new approach. *J. Geol.* **111**, 125–148 (2003).

4. J. Alroy, Colloquium paper: Dynamics of origination and extinction in the marine fossil record. *Proc. Natl. Acad. Sci. U.S.A.* **105** (suppl. 1), 11536–11542 (2008).

5. J. Alroy, A more precise speciation and extinction rate estimator. *Paleobiology* **41**, 633–639 (2015).

6. B. Kröger, F. Franeck, C. M. Ø. Rasmussen, The evolutionary dynamics of the early Palaeozoic marine biodiversity accumulation. *Proc. Biol. Sci.* **286**, 20191634 (2019).

7. Á. T. Kocsis, C. J. Reddin, J. Alroy, W. Kiessling, The r package divDyn for quantifying diversity dynamics using fossil sampling data. *Methods Ecol. Evol.* **10**, 735–743 (2019).

8. J. Alroy et al., Effects of sampling standardization on estimates of Phanerozoic marine diversification. *Proc. Natl. Acad. Sci. U.S.A.* **98**, 6261–6266 (2001).

9. R. K. Bambach, A. H. Knoll, S. C. Wang, Origination, extinction, and mass depletions of marine diversity. *Paleobiology* **30**, 522–542 (2004).

10. S. Finnegan, J. L. Payne, S. C. Wang, The Red Queen revisited: Reevaluating the age selectivity of Phanerozoic marine genus extinctions. *Paleobiology* **34**, 318–341 (2008).

11. J. L. Payne, S. Finnegan, The effect of geographic range on extinction risk during background and mass extinction. *Proc. Natl. Acad. Sci. U.S.A.* **104**, 10506–10511 (2007).

12. S. E. Peters, M. Foote, Determinants of extinction in the fossil record. *Nature* **416**, 420–424 (2002).

13. S. E. Peters, Environmental determinants of extinction selectivity in the fossil record. *Nature* **454**, 626–629 (2008).

14. J. L. Payne, A. Bachan, N. A. Heim, P. M. Hull, M. L. Knope, The evolution of complex life and the stabilization of the Earth system. *Interface Focus* **10**, 20190106 (2020).

15. E. A. Sperling et al., Statistical analysis of iron geochemical data suggests limited late Proterozoic oxygenation. *Nature* **523**, 451–454 (2015).

16. T. W. Dahl et al., Devonian rise in atmospheric oxygen correlated to the radiations of terrestrial plants and large predatory fish. *Proc. Natl. Acad. Sci. U.S.A.* **107**, 17911–17915 (2010).

17. W. Lu et al., Late inception of a resiliently oxygenated upper ocean. *Science* **361**, 174–177 (2018).

18. M. W. Wallace et al., Oxygenation history of the Neoproterozoic to early Phanerozoic and the rise of land plants. *Earth Planet. Sci. Lett.* **466**, 12–19 (2017).

19. D. A. Stolper, C. B. Keller, A record of deep-ocean dissolved O_2 from the oxidation state of iron in submarine basalts. *Nature* **553**, 323–327 (2018).

20. E. A. Sperling et al., A long-term record of early to mid-Paleozoic marine redox change. *Sci. Adv.* **7**, eabf4382 (2021).

21. A. J. Krause et al., Stepwise oxygenation of the Paleozoic atmosphere. *Nat. Commun.* **9**, 4081 (2018).

22. T. M. Lenton, S. J. Daines, B. J. W. Mills, COPSE reloaded: An improved model of biogeochemical cycling over Phanerozoic time. *Earth Sci. Rev.* **178**, 1–28 (2018).

23. R. Tostevin, B. J. W. Mills, Reconciling proxy records and models of Earth's oxygenation during the Neoproterozoic and Palaeozoic. *Interface Focus* **10**, 20190137 (2020).

24. E. A. Sperling, C. A. Frieder, L. A. Levin, Biodiversity response to natural gradients of multiple stressors on continental margins. *Proc. Biol. Sci.* **283**, 20160637 (2016).

25. E. Sampaio et al., Impacts of hypoxic events surpass those of future ocean warming and acidification. *Nat. Ecol. Evol.* **5**, 311–321 (2021).

26. L. A. Levin, "Oxygen minimum zone benthos: Adaptation and community response to hypoxia" in *Oceanography and Marine Biology: An Annual Review, Volume 41*, R.N. Gibson, R.J.A. Atkinson, Eds. (CRC Press, 2003), pp. 1–45.

27. H. O. Pörtner, A. P. Farrell, Ecology. Physiology and climate change. *Science* **322**, 690–692 (2008).

28. H. O. Pörtner, Oxygen- and capacity-limitation of thermal tolerance: A matrix for integrating climate-related stressor effects in marine ecosystems. *J. Exp. Biol.* **213**, 881–893 (2010).

29. C. Deutsch, A. Ferrel, B. Seibel, H. O. Pörtner, R. B. Huey, Ecophysiology. Climate change tightens a metabolic constraint on marine habitats. *Science* **348**, 1132–1135 (2015).

30. E. M. Howard et al., Climate-driven aerobic habitat loss in the California Current System. *Sci. Adv.* **6**, eaay3188 (2020).

31. M. I. Duncan, N. C. James, W. M. Potts, A. E. Bates, Different drivers, common mechanism; the distribution of a reef fish is restricted by local-scale oxygen and temperature constraints on aerobic metabolism. *Conserv. Physiol.* **8**, a090 (2020).

32. T. H. Boag, W. Gearty, R. G. Stockey, Metabolic tradeoffs control biodiversity gradients through geological time. *Curr. Biol.* **31**, 2906–2913.e3 (2021).

33. J. L. Penn, C. Deutsch, J. L. Payne, E. A. Sperling, Temperature-dependent hypoxia explains biogeography and severity of end-Permian marine mass extinction. *Science* **362**, eaat1327 (2018).

34. C. J. Reddin, P. S. Nätscher, Á. T. Kocsis, H. O. Pörtner, W. Kiessling, Marine clade sensitivities to climate change conform across timescales. *Nat. Clim. Chang.* **10**, 249–253 (2020).

35. T. H. Boag, R. G. Stockey, L. E. Elder, P. M. Hull, E. A. Sperling, Oxygen, temperature and the deep-marine stenothermal cradle of Ediacaran evolution. *Proc. Biol. Sci.* **285**, 20181724 (2018).

36. C. T. Reinhard, N. J. Planavsky, S. L. Olson, T. W. Lyons, D. H. Erwin, Earth's oxygen cycle and the evolution of animal life. *Proc. Natl. Acad. Sci. U.S.A.* **113**, 8933–8938 (2016).

37. E. A. Sperling, A. H. Knoll, P. R. Girguis, The ecological physiology of Earth's second oxygen revolution. *Annu. Rev. Ecol. Evol. Syst.* **46**, 215–235 (2015).

38. C. Deutsch, J. L. Penn, B. Seibel, Metabolic trait diversity shapes marine biogeography. *Nature* **585**, 557–562 (2020).

39. A. Ridgwell et al., Marine geochemical data assimilation in an efficient Earth system model of global biogeochemical cycling. *Biogeosciences* **4**, 87–104 (2007).

40. C. J. Reddin, Á. T. Kocsis, W. Kiessling, Climate change and the latitudinal selectivity of ancient marine extinctions. *Paleobiology* **45**, 70–84 (2019).

41. E. E. Saupe et al., Extinction intensity during Ordovician and Cenozoic glaciations explained by cooling and palaeogeography. *Nat. Geosci.* **13**, 65–70 (2020).

42. K. M. Meyer, A. Ridgwell, J. L. Payne, The influence of the biological pump on ocean chemistry: Implications for long-term trends in marine redox chemistry, the global carbon cycle, and marine animal ecosystems. *Geobiology* **14**, 207–219 (2016).

43. M. Gutjahr et al., Very large release of mostly volcanic carbon during the Palaeocene-Eocene Thermal Maximum. *Nature* **548**, 573–577 (2017).

44. G. L. Foster, D. L. Royer, D. J. Lunt, Future climate forcing potentially without precedent in the last 420 million years. *Nat. Commun.* **8**, 14845 (2017).

45. S. N. C. Woolley et al., Deep-sea diversity patterns are shaped by energy availability. *Nature* **533**, 393–396 (2016).

46. E. A. Sperling, R. G. Stockey, The temporal and environmental context of early animal evolution: Considering all the ingredients of an "explosion". *Integr. Comp. Biol.* **58**, 605–622 (2018).

47. B. A. Seibel, C. Deutsch, Oxygen supply capacity in animals evolves to meet maximum demand at the current oxygen partial pressure regardless of size or temperature. *J. Exp. Biol.* **223**, jeb.210492 (2020).

48. T. W. Hearing et al., An early Cambrian greenhouse climate. *Sci. Adv.* **4**, eaar5690 (2018).

49. J. A. Trotter, I. S. Williams, C. R. Barnes, C. Lécuyer, R. S. Nicoll, Did cooling oceans trigger Ordovician biodiversification? Evidence from conodont thermometry. *Science* **321**, 550–554 (2008).

50. S. L. Goldberg, T. M. Present, S. Finnegan, K. D. Bergmann, A high-resolution record of early Paleozoic climate. *Proc. Natl. Acad. Sci. U.S.A.* **118**, e2013083118 (2021).

51. C. Vérard, J. Veizer, On plate tectonics and ocean temperatures. *Geology* **47**, 882–885 (2019).

52. B. J. W. Mills et al., Modelling the long-term carbon cycle, atmospheric CO_2, and Earth surface temperature from late Neoproterozoic to present day. *Gondwana Res.* **67**, 172–186 (2019).

53. K. D. Bergmann et al., A paired apatite and calcite clumped isotope thermometry approach to estimating Cambro-Ordovician seawater temperatures and isotopic composition. *Geochim. Cosmochim. Acta* **224**, 18–41 (2018).

54. R. A. Close, R. B. J. Benson, E. E. Saupe, M. E. Clapham, R. J. Butler, The spatial structure of Phanerozoic marine animal diversity. *Science* **368**, 420–424 (2020).

55. A. R. Palmer, Trilobites of the Late Cambrian pterocephaliid biomere in the Great Basin, United States. *U.S. Geol. Surv. Prof. Pap.* **493**, 1–104 (1965).

56. A. R. Palmer, The biomere problem: Evolution of an idea. *J. Paleontol.* **58**, 599–611 (1984).

57. R. A. Fortey, There are extinctions and extinctions: Examples from the lower Palaeozoic. *Philos. Trans. R. Soc. Lond. B Biol. Sci.* **325**, 327–355 (1989).

58. M. R. Saltzman, C. T. Edwards, J. M. Adrain, S. R. Westrop, Persistent oceanic anoxia and elevated extinction rates separate the Cambrian and Ordovician radiations. *Geology* **43**, 807–810 (2015).

59. B. C. Gill et al., Geochemical evidence for widespread euxinia in the later Cambrian ocean. *Nature* **469**, 80–83 (2011).

60. M. Elrick, S. Rieboldt, M. Saltzman, R. M. McKay, Oxygen-isotope trends and seawater temperature changes across the Late Cambrian Steptoean positive carbon-isotope excursion (SPICE event). *Geology* **39**, 987–990 (2011).

61. M. A. LeRoy, B. C. Gill, E. A. Sperling, N. R. McKenzie, T.-Y. S. Park, Variable redox conditions as an evolutionary driver? A multi-basin comparison of redox in the middle and later Cambrian oceans (Drumian-Paibian). *Palaeogeogr. Palaeoclimatol. Palaeoecol.* **566**, 110209 (2021).

62. A. Y. Zhuravlev, R. A. Wood, Anoxia as the cause of the mid-Early Cambrian (Botomian) extinction event. *Geology* **24**, 311–314 (1996).

63. W. Yao, A. Paytan, U. G. Wortmann, Large-scale ocean deoxygenation during the Paleocene-Eocene Thermal Maximum. *Science* **361**, 804–806 (2018).

64. H. C. Jenkyns, Geochemistry of oceanic anoxic events. *Geochemis. Geophys. Geosyst.* **11** (2010).

65. M. O. Clarkson et al., Uranium isotope evidence for two episodes of deoxygenation during Oceanic Anoxic Event 2. *Proc. Natl. Acad. Sci. U.S.A.* **115**, 2918–2923 (2018).

66. D. H. Erwin, Lessons from the past: Biotic recoveries from mass extinctions. *Proc. Natl. Acad. Sci. U.S.A.* **98**, 5399–5403 (2001).

67. A. H. Knoll, Systems paleobiology. *Bull. Geol. Soc. Am.* **125**, 3–13 (2013).

68. A. H. Knoll, R. K. Bambach, J. L. Payne, S. Pruss, W. W. Fischer, Paleophysiology and end-Permian mass extinction. *Earth Planet. Sci. Lett.* **256**, 295–313 (2007).

69. J. L. Payne, M. E. Clapham, End-permian mass extinction in the oceans: An ancient analog for the twenty-first century? *Annu. Rev. Earth Planet. Sci.* **40**, 89–111 (2012).

70. J. X. Fan et al., A high-resolution summary of Cambrian to Early Triassic marine invertebrate biodiversity. *Science* **367**, 272–277 (2020).

71. A. Mehra et al., Curation and analysis of global sedimentary geochemical data to inform earth history. *GSA Today* **31**, 4–9 (2021).

72. Ú. C. Farrell et al., The sedimentary geochemistry and paleoenvironments project. *Geobiology*, 10.1111/gbi.12462 (2021).

73. K. W. Flessa, D. Jablonski, Declining Phanerozoic background extinction rates: Effect of taxonomic structure? *Nature* **313**, 216–218 (1985).

74. K. M. Meyer, A. Ridgwell, Biogeochemical controls on photic-zone euxinia during the end-Permian mass extinction. *Geology* **36**, 747–750 (2008).

75. A. Pohl et al., Glacial onset predated Late Ordovician climate cooling. *Paleoceanography* **31**, 800–821 (2016).

76. D. O. Gough, Solar interior structure and luminosity variations. *Sol. Phys.* **74**, 21–34 (1981).

77. A. F. Hofmann, E. T. Peltzer, P. M. Walz, P. G. Brewer, Hypoxia by degrees: Establishing definitions for a changing ocean. *Deep. Res. Part I Oceanogr. Res. Pap.* **58**, 1212–1226 (2011).

78. C. T. Edwards, M. R. Saltzman, D. L. Royer, D. A. Fike, Oxygenation as a driver of the Great Ordovician Biodiversification Event. *Nat. Geosci.* **10**, 925–929 (2017).

8 of 8 | **PNAS**
https://doi.org/10.1073/pnas.2101900118

Stockey et al.
Decreasing Phanerozoic extinction intensity as a consequence of Earth surface oxygenation and metazoan ecophysiology